Relative Abundances of Elements ($20 \leq Z \leq 28$) at Energies up to 70GeV/amu Using Relativistic Rise in Ion Chambers

S.D. Barthelmy [1], *M.H. Israel, J. Klarmann*

Physics Department and McDonnell Center for the Space Sciences
Washington University, St. Louis, Missouri 63130, USA

1. Introduction This paper reports on the results of a new balloon borne cosmic ray detector flown from Palestine, TX in Sept 1982. The exposure of 62 m^2-ster-hr is sufficient to prove the concept of using gas ionization chambers as energy measuring devices in the relativistic rise region. We have measured the abundances, relative to $_{26}$Fe, of the pure secondaries $_{22}$Cr and $_{24}$Ti, the pure primary $_{28}$Ni, and the mixed primary and secondary $_{20}$Ca between 6 and 70GeV/amu.

2. Instrument The instrument, shown in figure 1, is composed of 1.0cm NE114 plastic scintillator(**S**), and 0.6cm Pilot 425 plastic Cherenkov(**P**), detectors in light diffusion boxes. These two detectors determine the charge of the cosmic rays. Interspaced around the **S** and **P** detectors are pairs of 10cm dual gap P-10 gas ionization chambers(**I**). In addition to being the energy measuring devices they are also used for identification of nuclear interactions in **S** and **P** detectors. At the bottom of the stack is a one atmosphere CO_2 gas Cherenkov(**G**), whose nominal threshold energy is 34.8GeV/amu. This detector provides the energy calibration of the relativistic rise region of the ion chambers. The two layers of x-y multiwire ionization hodoscopes(**H**) provide the trajectory information which allows for the path length correction and for correction to the areal variations of the various detectors. The stack, 160cm x 160cm x 190cm, with the electronics is flown inside a one atmosphere pressure vessel.

Figure 1

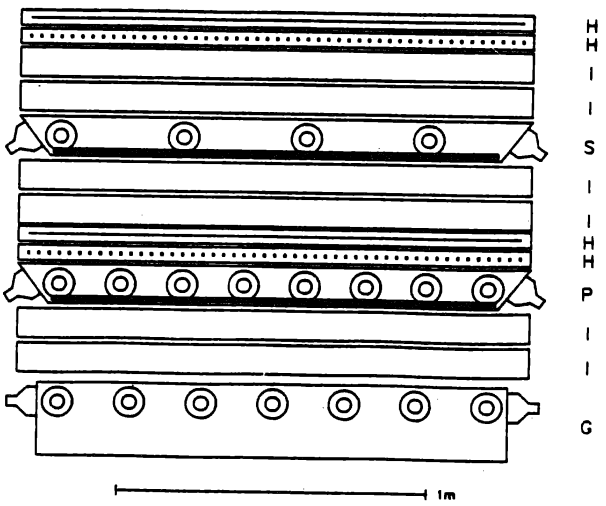

3. Data Reduction Figure 2 is a plot of the mean ionization signal(**I**) versus the plastic Cherenkov signal(**P**). The dashed lines are the charge tracks for the even Z elements 20 to 28. The vertical pairs of lines mark the β=1 saturation of **P**, the events of interest in this experiment. With **I** and **P** alone it is impossible to separate, say, relativistically risen charge 24 from low energy charge 26. To remove this ambiguity a third dimension, scintillation(**S**), is added.

[1] Presently at Goddard Space Flight Center, Greenbelt, Maryland 20771, USA

Figure 3 is a plot of the same events for **S** versus **P**. The energy dependence is almost entirely in the **P** dimension. The relativistic events pile up at the right side of the cluster and lower energy events trail off towards the left. The superposed boxes are the **S** and **P** cuts used to select events that will be used to form abundance spectra. We observe that **S** has negligible (less than 0.5%) relativistic rise at 100GeV/amu, so the **S** cuts do not introduce a significant energy dependence.

Figure 2

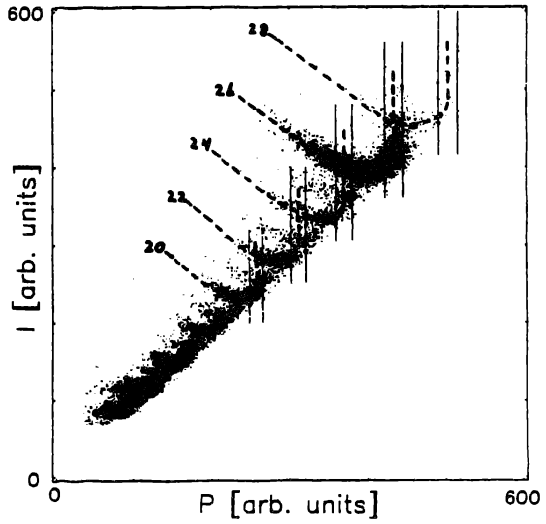

Figure 3

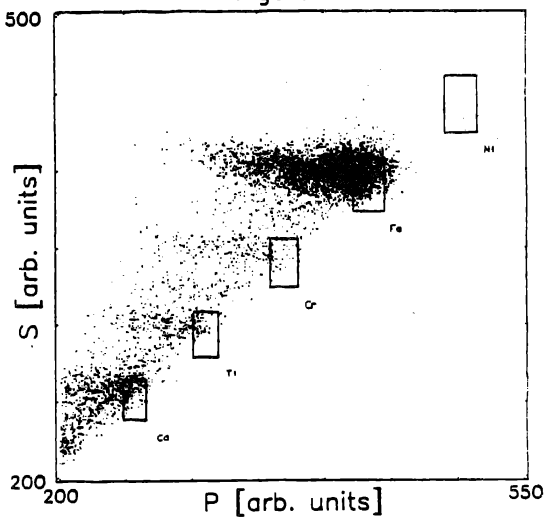

The **S** cuts are asymmetric about the charge tracks. This is because almost all the contamination from adjacent charges into a given charge selection box is from the lower energy next higher charge. The **P** cuts are symmetric about the β=1 track of the given charge. Both the **S** and **P** cuts are made in constant sigma units for each charge. This insures a constant fraction of the desired charge to be included within the **S-P** box cuts. Taking the events within these cuts, histograms were formed in $\mathbf{I/I_{min}}$. Ratios of these histograms to that for iron are the abundance ratio spectra that are discussed in section 5.

4. Energy Calibration Figure 4 is a plot of **I** vs **G** for the events satisfying the **S** and **P** cuts in figure 3 for iron. The line through the data is a result of a least-squares fitting with the semi-empirical model described by equations 1.

$$I = I_m \ln(E) + B \qquad (1a)$$

$$G = K(1 - E_{thresh}^2/E^2) + D \qquad (1b)$$

I is the ratio of the **I** signal over the minimum value (at 2.4GeV/amu). The D term represents the scintillation emission from the reflective paint coating on the inside of the **G** light diffusion box.

The fitting was done in two steps. The first attempt only fit the events between the **G** values of 450 and 1100. Using this fit a swath through **I** and **G**

Figure 4

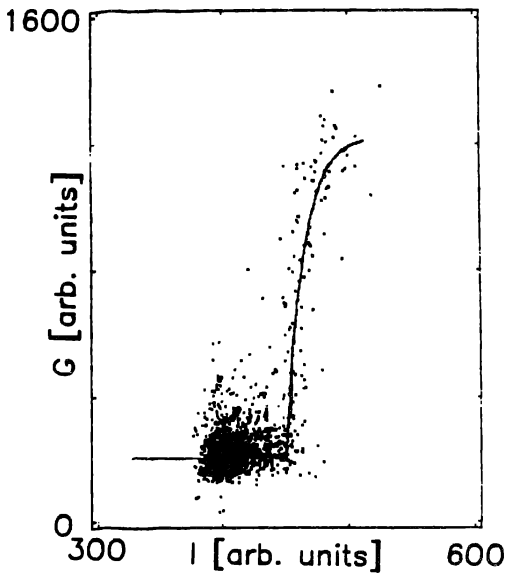

space was made to allow for the inclusion of events down beside the paint emission clump and to extend the high end to include the β=1 events in the **G** detector. The sharp threshold in **G** can be seen and it is the **I** value at this E_{thresh} that provides one well defined calibration point. Given the limited number of events the slope (Im) was very poorly determined from this **I** vs **G** comparison, and so we instead determined the slope by comparison between our iron data and the iron spectrum from previous experiments (summarized by Webber[1]).

For various values of Im, with B selected to give the previously determined $\mathbf{I}(E_{thresh})$, we convolved the Webber spectrum with equation 1 and with the resolution function of the detector. We then determined the value of Im which gave the best least-squares fit to our observed **I**-spectrum for iron. The final values of the parameters in equation 1 are I_m = 0.0738 ± 0.0023, B = 0.8889 ± 0.0019, K = 1220.0 ± 15, and D = 207.0 ± 4.0. The numerical values of the parameters for equation 1a apply to an **I** scale in which minimum-ionizing iron gives **I**=1.000, and this equation is taken as applicable for energies greater than 5.0 GeV/amu.

5. Results Even with the tight **S** cuts near the Z+1 charge track, there is still some contamination. While these contamination events are of low intrinsic energy, their **I** mimics relativisticly risen events because they have a greater charge. The upper **S** cut was fixed by requiring that the contamination to any of the five charges never be more than 20% of the charge of interest at the appropriate $\mathbf{I}/\mathbf{I}_{min}$ value. Subtractions were made for these contaminations. After producing the number versus $\mathbf{I}/\mathbf{I}_{min}$ spectra, they are binned into three differential points, one integral point, and using similar **S** and **P** cuts, a point at $\mathbf{I}_{min}$ (2.4GeV/amu).

Our results are listed in table 1 and plotted (points with error bars) in figure 5. In the energy interval 6 to 25 GeV/amu our results are consistent with those of Englemann[2] (their data has been propagated through 4.1 g/cm^2 of air). Above 25 GeV/amu our results indicate an energy dependence of relative abundances which continues the trend observed by Englemann, et al.

TABLE 1 - Abundance Ratios to Iron for Ti, Cr, Ca, and Ni

Energy Range		Element			
Lower	Upper	Ti	Cr	Ca	Ni
~1.45	~3.35	0.158 ± 0.007	0.161 ± 0.007	0.217 ± 0.009	0.055 ± 0.004
5.90	11.62	0.129 ± 0.013	0.124 ± 0.013	0.225 ± 0.018	0.052 ± 0.008
11.62	22.87	0.101 ± 0.023	0.086 ± 0.021	0.178 ± 0.032	0.037 ± 0.014
22.87	45.02	0.059 ± 0.023	0.074 ± 0.026	0.092 ± 0.029	0.034 ± 0.017
45.02	∞	0.070 ± 0.023	0.075 ± 0.024	0.126 ± 0.032	0.043 ± 0.018

6. Acknowledgements We are grateful to W. R. Webber for valuable suggestions regarding the design of this experiment, and to John Epstein and John Vogel for essential contributions to the construction of the instrument. This work was supported in part by NASA grant NGR-26-008-001.

References:

[1] Webber, W.R, 1982 Erice NATO Conference, 1983, Reidel, pp 25-45
[2] Englemann J.J., et al, 1983, ICRC, Bangalore, India, OG1-9, pp 17

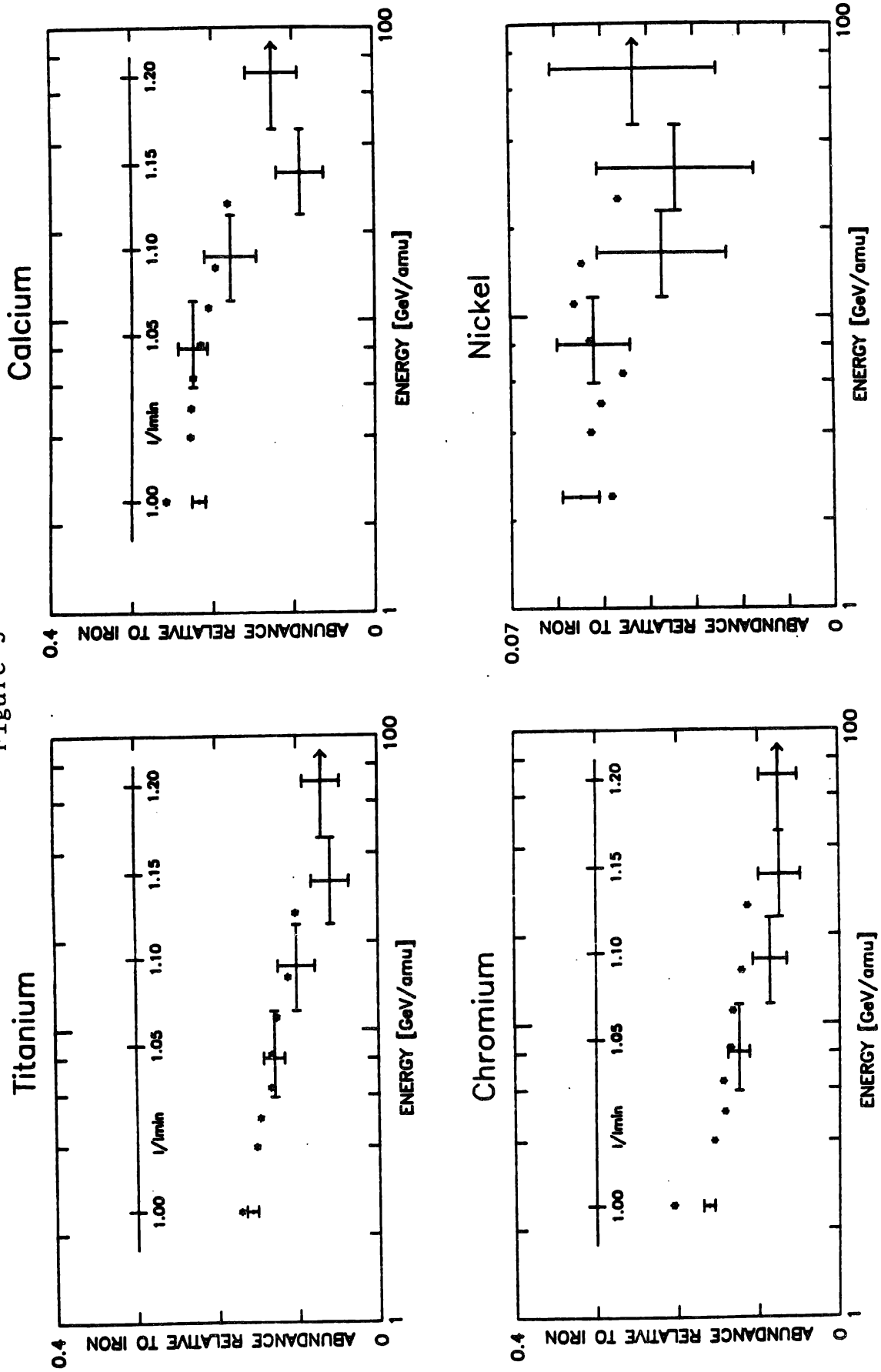

Figure 5